Omnidirectional Free Space Detection using Contour Active with Riemannian Metric

Jamal Mirhisse
LABO MATSI, ESTO, B.P
473,University Mohammed I
Oujda, Maroc.

M'Barek Nasri
LABO MATSI, ESTO, B.P
473,University Mohammed I
Oujda, Maroc.

Abdelmajid Essadqui
LABO MATSI, ESTO, B.P
473,University Mohammed I
Oujda, maroc.

Djemaa Kachi
Labo Mis
University of Picardie Jules Verne
Amiens, France

ABSTRACT
The direct classic processing on the catadioptric images end in errors. The latter are related mainly to the difference in the resolution of the omnidirectional images that is raised up to the periphery and weak in the center of the image. In this paper, we propose a solution, based on a model of parametric active contour in Riemannian metric, which is adapted for the catadioptric images. This model of active contour is designed for the extraction of the free space, which will allow establishing a system of autonomous navigation of a mobile robot in real time. The approach adopted here is compared with methods of classic active contours.

KEYWORDS
Omnidirectional vision, active contours, free space, Riemannian metric.

1. INTRODUCTION
The omnidirectional vision [4] is the process of vision which supplies a sphere of worldview observed from its center. It has become essential for the navigation of the mobile robots, because it offers a large field of view and complete information about the world surrounding the robot that allows an autonomous and secure navigation. Numerous approaches have been proposed in the literature to detect free space, usually based on movement estimation. The works [10][7] have developed algorithms able to detect free space in an omnidirectional image sequence by estimating the optical flow. However, these methods require knowledge of the environment and assumptions made on the camera motion to correctly perform the extraction. Furthermore, the omnidirectional images contain important distortions due to the geometry of the mirror. These distortions have then significant repercussions on the possible processing and the direct application of conventional operators that cannot offer satisfactory results. Then, the methods of approximation of free space [4], cannot be directly used for the omnidirectional vision. In this regard, to have a system of detection of free space adapted for catadioptric images, the mirror geometry of the catadioptric sensor must be taken into account.

In this paper we propose a solution based on a model of active outline parameterized in Riemannian metrics, adapted for the catadioptric images and which takes into account the geometry of mirror. This model is the adaptation of the initial model [4] for the catadioptric images. The metrics, which is used to deform artificially the image, is calculated so that the precision is highly possible in the central area of the image. This metrics is directly determined from the mirror geometry of the catadioptric sensor. The idea is to replace the Euclidian corresponding distance by a non-conforming metrics dependent on information presented in the image. This defines Riemannian metrics in the domain of the image domain, where the limits of the target objects to be detected appear as closed geodesic curves. Comparative results obtained from synthetic images and omnidirectional images in a real environment are taken to evaluate and validate our approach.

This paper is structured around three main sections. In1st section, we define the model of active contour which is used to segment omnidirectional free space and present the chosen numerical approximations of its snake functional energies. The 2nd section is devoted to calculate the Riemannian metric which will be used to parameterize the model of active contour which we have chosen. The last section shows the comparative results between the parametric model and the classic model, by way of which this study will be brought to conclusion.

2. ACTIVE CONTOUR MODEL
The navigating environment of a robot in movement is typically a deformable space, where the use of the models of deformable contour was imperative. The original model of the active contour was proposed by Kass and al. [9] and consists of an intrinsically closed deformable model which evolves towards the borders of the desirable region. The deformation is established on a Lagrangian formulation of the energy minimization, referred to as the sum of a term attached to the image data and as a term of regularization. Many studies have been conducted to make the pursuit of a deformable object in an image sequence. All these studies differ in terms of the deformation model [8][13][14].

The functional which we try to minimize is the same one in the original model [12][11] which we are going to adapt in a Riemannian space.

2.1 Parametric Active Contour
Because the snake can form a made up graph, we can represent it in a parametric form [1] by:

$$v \coloneqq [0,1] \to IR^2$$

The active contour can be described by a curve $\boldsymbol{C}$, function of time $\boldsymbol{t}$ and of the curvilinear abscissa $\boldsymbol{s}$ as the following formula shows:

$$C = \{v(s,t) = (x(s,t), y(s,t)) \,/\, s \in [a,b], t \in [0,1]\}$$

Where a and b represent the extremities of the snake (Figure 1)

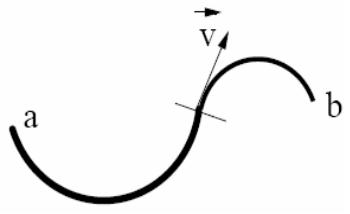

Fig 1: Curve C

The functional of energy of the snake with whose minimization will control the evolution of $v(s)$is defined by:

$$E(v) = \int_0^1 \alpha E_{cont}(v(s)) + \beta E_{curv}(v(s)) + \gamma E_{grad}(v(s)) + \delta E_{ball}(v(s))ds \quad (1)$$

By α, β, δ and γ are meant constant weighting parameters used to balance the relative influence of the local energies. The first three ones are positive and the last one is negative to allow a balance between the intrinsic geometrical data of the snake, and the extrinsic image data.

E_{cont} energy is the continuity term that controls the snake bending. It is expressed as a function of the first order derivative of v as to s, $E_{cont} = |v'(s)|^2$. E_{curv} energy is the curvature term that controls the snake rigidity. It is defined as a function of the second-order derivative of v according to s, $E_{curv} = |v''(s)|^2$. E_{ball} energy expresses a pressure force and is defined as $E_{ball} = \vec{n}$ where $\vec{n}$ is the normal to the snake at a snake point. It allows the snake to overpass local minima as in the initial state or in homogeneous image gradient areas. Notice that, these three terms only take into account intrinsic characteristics of the contour.

Finally,E_{grad} represents the image forces. Given a gray level image $I(x,y)$, viewed as a function of continuous position variables *(x,y)*,the image force chosen to lead an active contour toward step edges is $E_{grad} = -|\nabla I|^2$. The negative sign is important as it will ensure an equilibrium between intrinsic contour forces and the image ones, and thus converge the snake to salient image edges.

The equation (1) could then be written as follows:

$$E(v) = \int_0^1 [\alpha|v'(s)|^2 + \beta|v''(s)|^2 - \gamma|\nabla I|^2 + \delta\vec{n}]\,ds \quad (2)$$

2.2 Formulation of the Energies

The deformation of the active contour is made by an iterative plan using a discreet approximation of the functional of continuous energy (1). [6] proved that iterative methods are less time-consuming than other numerical approaches using dynamic programming or variational calculus.

We denote V^k the set of$n$points which compose the active contour at the iteration$k$. $V^k(i)$ is the i^{th} point of the contour, and $V_v^k(i) = \{V_j^k(i), j = 1 \dots 8\}$ the eight-neighbor points of the snake point $V^k(i)$ in the domain image.

We propose to approximate the continuity term E_{cont} and the curvature term E_{curv} expressed respectively by the first and the second-order contour derivatives in equation (2), using centered finite differences:

$$E_{cont} = \left|\frac{\partial V^k(i)}{\partial s}\right|^2 \simeq \frac{|V^k(i+1) - V^k(i-1)|^2}{(h_{i+1} + h_{i-1})} \quad (3)$$

$$E_{curv} = \left|\frac{\partial^2 V^k(i)}{\partial^2 s}\right|^2 \simeq \frac{|V^k(i+1) + V^k(i-1) - 2V^k(i)|^2}{(h_{i+1} h_{i-1})} \quad (4)$$

Where h_{i+1} (respectively h_{i-1}) is the distance between $V^k(i+1)$ (respectively $V^k(i-1)$) and$V^k(i)$

The balloon energy E_{ball} is the normal to the curve C at the snake point $V^k(i)$. It is approximated locally using the coefficients of the line joining $V^k(i+1)$ and $V^k(i-1)$. The image forces E_{grad} are computed in each pixel of the image using a Canny detector.

The functional of the energy of the snake is evaluated at each snake point $V^k(i)$ and each of its eight neighbors. The location having the smallest energy value is chosen as a new position of $V^k(i)$ The process is repeated until convergence, i.e, until the contour at iteration k+1 and k are the same to an epsilon.

In the Riemannian variety, the equations of the energy must consider the metric. All the calculations are made by Riemannian measures. The model does not locally realize that it evolves in a deformed space. The Forces are thus adapted to the Riemannian measures. The elastic and rigidity forces are materialized by springs. The extension of springs is thus naturally measured with the Riemannian metrics. Also, the external forces are too renormalized to take into account the metric.

3. RIEMANNIAN METRIC

The distortion in the omnidirectional images caused by the mirror geometry raises the problem of irregularity of the distances between points in the images space, thus to apply a direct processing to this type of images it is necessary to define a new distance which takes into account the geometrical properties of the mirror surface. These properties are encoded in its induced Riemannian metricg_{ij} : An application which is in any point *(x, y)* of the plan associated to a scalar product $g_{(x,y)}$ on $\mathbb{R}^2$. This scalar product provides a way to measure vectors: length of a movement $\overrightarrow{dl} = (dx, dy)$ can be written $g_{(x,y)}(\overrightarrow{dl}, \overrightarrow{dl})^{\frac{1}{2}}$

The Riemannian geometry was already used in the context of the deformable models, in particular to define the active contour or the geodesic active surfaces [2][5] as the minimal paths in space deformed by the image.

3.1 Calculus of the metric

We present a method for detecting free space on the catadioptric images, taking into consideration mirror geometry of the sensor while remaining in the image plane, which is to work in Cartesian coordinates on image plane without making a priori projections for changed space [5].

Let (x, y) and (x_0, x_1, x_2) label coordinates in the image plane, here an open subset $\Omega \subseteq \mathbb{R}^2$, and on the mirror surface $\mathcal{M}$on $\mathbb{R}^3$, respectively. The whole catadioptric image formation process depicted above induces a mapping between manifolds from the surface of the mirror to the camera plane:

$$\phi: \mathcal{M} \to \Omega$$

$$(x_0, x_1, x_2) \to (x, y)$$

In this paper we focus only on parabolic mirrors, the steps are similar for the other types of the mirror. The reader interested in details can be referred to [3].

[5] Showed that the calculation of the metrics via the polar coordinates gives a non-diagonal metric which will be a source of complication, so we will use the spherical coordinates to move from the mirror surface to the image plane.

Consider a sphere of radius r as depicted in figure 2, a point on the sphere is identified with the vector: $(x_0, x_1, x_2) = (rcos\theta, rsin\theta cos\varphi, rsin\theta sin\varphi),\ \theta \in [0,\pi] et \varphi \in [0,2\pi]$

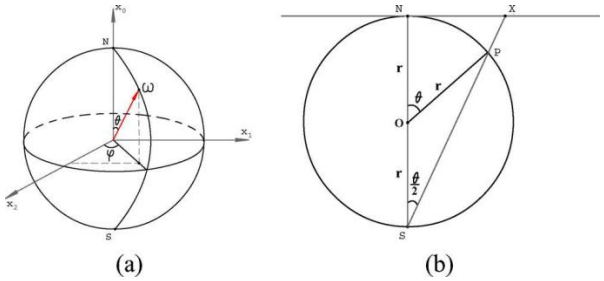

Fig 2: Geometry of the sphere, (a) spherical polar coordinates and (b) stereographic projection.

By using a system of spherical coordinate (r, φ) (figure 2), the elementary Euclidian movement is given by:

$$dl^2 = dx_0^2 + dx_1^2 + dx_2^2 = d\rho^2 + \rho^2(d\theta^2 + sin^2\theta d\varphi^2) \quad (5)$$

On the surface $\rho = r$ and the differential $d\rho = 0$, so the metric induced on the sphere is given by the well-known expression:

$$dl^2 = r^2(d\theta^2 + sin^2\theta d\varphi^2) \quad (6)$$

The stereographic projection sends a point on the sphere (θ, φ)on the sphere to the point with polar coordinates to the point with polar coordinates (R, φ) in the plane, for which we have$R = \frac{r}{2}\tan\left(\frac{\theta}{2}\right)$. It is shown in figure 3. Interms of these new coordinates, the equation (6) becomes:

$$dl^2 = \frac{4r^2}{(r^2+R^2)^2}(dR^2 + R^2 d\varphi^2) \quad (7)$$

Let us pass toward coordinates on the disk $(x_1, x_2) \equiv (x, y) \in \mathbb{R}^2$,with $R^2 = x^2 + y^2$. We obtain:

$$dl^2 = \frac{4r^2}{(r^2+x^2+y^2)^2}(dx^2 + dy^2) \quad (8)$$

We notice well that in this case, the metric on the sphere is obtained by multiplying the Euclidian metrics by the function$\frac{4r^2}{(r^2+x^2+y^2)^2}$

$$dl^2_{\mathbb{S}^2} = \frac{4r^2}{(r^2+x^2+y^2)^2} dl^2_{\mathbb{R}^2} \quad (9)$$

Accordingly, the metric induced on $\mathbb{R}^2$ when $r = 1$ is direved as:

$$g_{ij}(x, y) = \begin{pmatrix} \frac{4}{(1+x^2+y^2)^2} & 0 \\ 0 & \frac{4}{(1+x^2+y^2)^2} \end{pmatrix} \quad (10)$$

And, consequently, the inverse metric is as follows:

$$g^{ij}(x, y) = \begin{pmatrix} \frac{(1+x^2+y^2)^2}{4} & 0 \\ 0 & \frac{(1+x^2+y^2)^2}{4} \end{pmatrix} \quad (11)$$

It is this metric which we are going to use to define our model of parametric active contour in Riemannian metric adapted to approximate the omnidirectional free space.

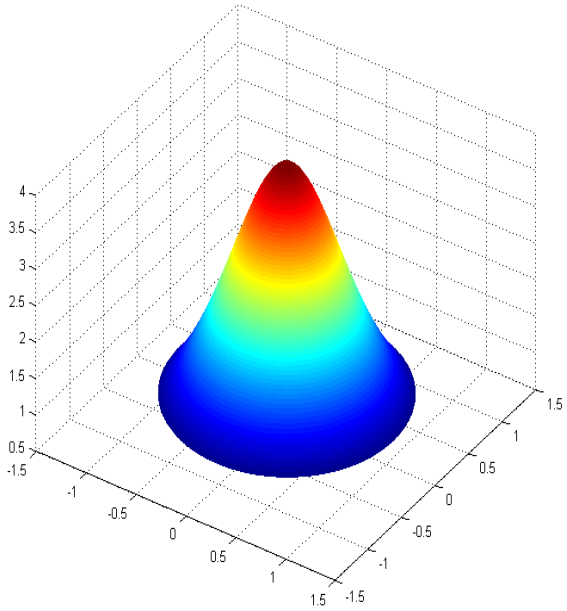

Fig 3: Graphical representation of the metric tensor h_{ij}

We notice clearly on the figure 3 that the appropriate values of the metric are so important at the image center which allows to enlarge the zone of the center of the image and to reduce the zone to the periphery.

3.2 Gradient Corrected with the Riemannian Metric

The gradient of a scalar function *I* is defined by:

$$D_v I = \nabla I.V$$

In Riemannian variety (M, g_{ij}) the directional derivative is replaced by a vector$v$tangent with plane of Mat a point p, the scalar product at this point is defined by the following metric:

$$V[I] = \langle \nabla I.V \rangle_p$$

In a system of coordinates x^i on M, the component of the gradient is written as follows:

$$\nabla^i = g^{ij}\frac{\partial}{\partial x^i} \quad (12)$$

By using the metric (11) and the equation (12), we deduct the expression of the parabolic gradient which is expressed by the following formula:

$$\nabla_D = \frac{(1+x^2+y^2)^2}{4}\nabla_{\mathbb{R}^2} \quad (13)$$

The figure 4, shows the detector of Canny normalized with the Riemannian metric applied to an omnidirectional image. The obtained result is a map of gradient in the grey level, of which the intensity varied according to the position in the image, contrary to the classic detector of Canny which gives a uniform gradient onto the entire image. In this way by using adapted thresholding we can eliminate the false positives which appear on the image, or to detect the lost false negatives.

(a)

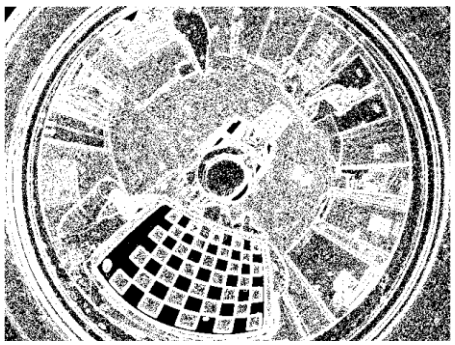

(b)

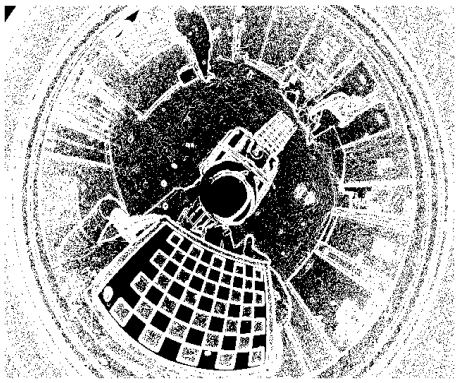

(c)

Fig 4: (a) catadioptric image ; (b) classic Canny detector; (c) corrected Canny detector.

3.3 Riemannian Distance

The exact calculation of Riemannian distance is a difficult problem and numerical algorithms of approximation are expensive. However, in our case we do not generally need to calculate the exact distance between two points since the points of the snake are quite close so it is reasonable to approximate the geodesic by a straight, that is why we adopted Lachaud's approach [2]; if we assume that the metrics varies linearly along this path, we obtain an approximation of the Riemannian distance between two points p and q such as:

$$d_R(p,q) = \frac{2\left(n_p^2 + n_p n_q + n_q^2\right)}{3\left(n_p + n_q\right)} \qquad (14)$$

Where n_p and n_q are the Riemannian norms of the vector pq taken respectively in points p and q.

4. RESULTS AND CONCLUSION

4.1 Discussion of Results

In this section we discuss the results of segmentation of free space obtained with our approach of active contour on synthetic images and real catadioptric images. We compare the performances of our active model of parametric contour in Riemannian metric with the classic model. Two criteria of comparison are used: (i) the number of the iterations is made by the snake algorithm to arrive at the convergence and (ii) the final shape of the snake is estimated visually and it describes the capacity of the active outline to correspond to the free space in the image.

At first we are going to present the results of the tests on synthetic images, of resolution 960 * 720 pixels and format JPG, with deferential form of space to be segmented. We pass later to the results of test on catadioptric images, of resolution 1280 * 960 pixels and format PNG, acquired by a mobile robot during an exploration guided in internal environments.

The figure 5 shows the results of approximation of the omnidirectional free space on synthetic images with the Euclidian model on the left and with our model of parametric active contour in Riemannian metrics on the right.

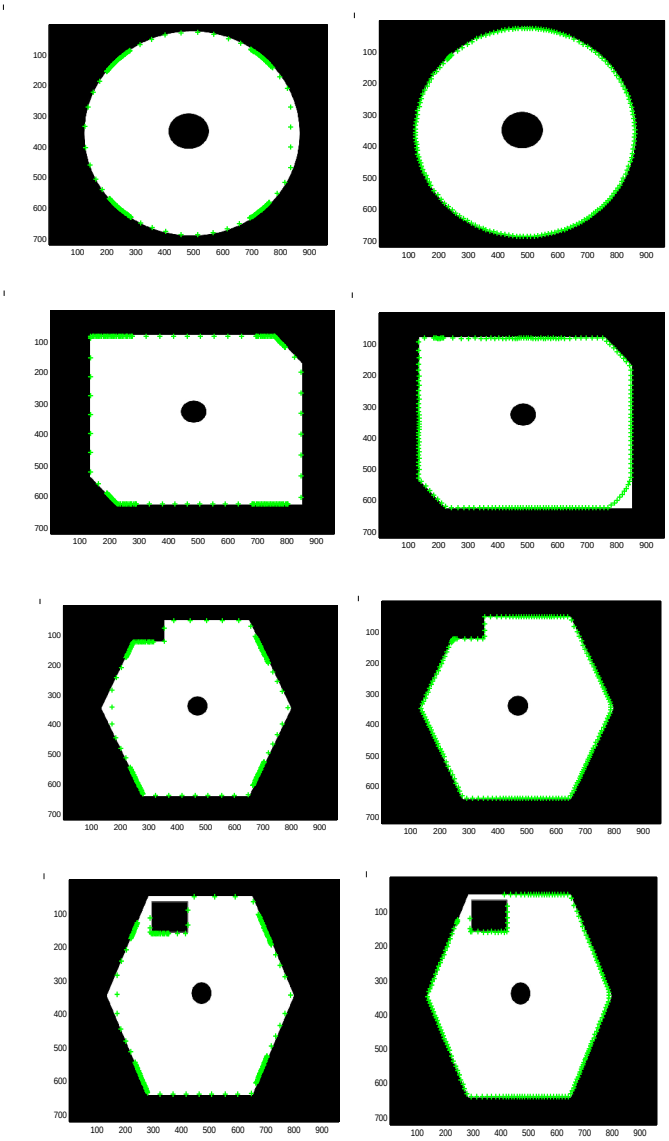

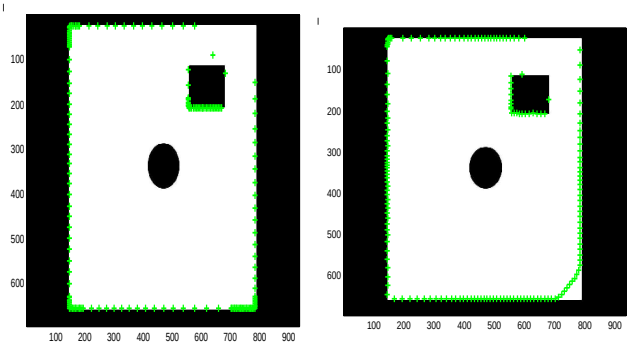

Fig 5: segmentation of free space in the synthetic images with classical Euclidean model (left column) and our Riemannian parametric model (right column).

In the figure 5 both models finish by converged after 350 iterations maximum, we notice well the large difference between the Euclidian classic model and our parametric model in Riemannian geometry, with our approach, we obtained a very good result of approximation of omnidirectional free space with a total stability of 150 points of the snake in all the synthetic images. The effect of the Riemannian metrics is very clear in the results: the equidistance between 150 points is well respected; in turn we notice the grouping of the points of the snake in the classical model. This is due to that our model evolves in a non-uniform space and that the Riemannian geometry is not isotropic.

The figure 6 shows the results of approximation of the omnidirectional free space, on catadioptric images taken in a real environment, with the Euclidian model to the left and with our model of parametric active contour in Riemannian metrics to the right.

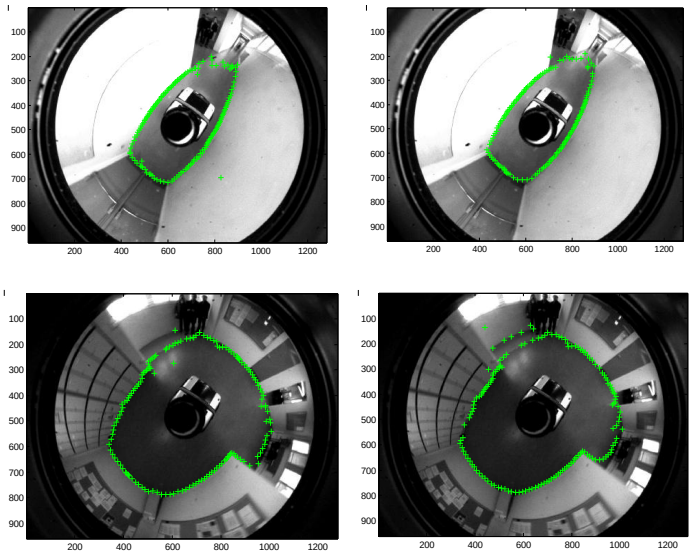

Fig 6: segmentation of omnidirectional free space in a real environment with classical Euclidian model (left column) and our Riemannian parametric model (right column).

Visually the results presented in the figure 6 seem coherent and correct for both models, they are able to adequately model an approximation of the omnidirectional free space. We tried to validate this visual impression through the comparison of our model with the initial model. For this reason, we used the criteria presented in the following board,

Table 1: execution time and the number of iteration of each method.

	Classical Euclidian model		our Riemannian parametric model	
	Run time (s)	number of iterations	Run time (s)	number of iterations
Fig.6 (a)	11.825 76	129	23.845 61	95
Fig.6 (b)	15.158 42	204	26.686 84	196

We can well notice that we have obtained a good segmentation of the free space as shown in fig. 6 by a little number of iterations made with our model than the iterations made with the initial model.
Besides, we underline that the difference between the time of execution of our Riemannian algorithm and the Euclidian classical algorithm is reasonable; this is due to a supplementary operation of correction.

4.2 Conclusion

In this work, we presented our approach of detection of contour and approximation of free space in the omnidirectional images and we compared it with the classic model of active contour. For this we tested our approach on real images and synthetic images with more complex forms, which contain concave or convex parts or obstacles. The results show the interest of our approach, which considers the geometry of the omnidirectional images. By replacing the Euclidian metrics with our Riemannian metric which is calculated from the geometry of the mirror, the zone of the center of the image is artificially enlarged in a way that allows our model to detect the contour of the present objects in this zone. This work is not finished yet, as perspective, we intend to reduce the time of segmentation of free space and to solve the problem of detection of falsely classified obstacles resultant of the light projection on the ground, and to face the problem of the obstacles in movement and allow the active contour to follow such an object in a sequence of omnidirectional image with robustness, the future work is to make the tracking of objects by active contour in a sequence of omnidirectional image

5. REFERENCES

[1] Fekir, N. Benamrane, and A. Taleb-Ahmed, "Détection et Suivi d'Objets dans une Séquence d'Images par Contours Actifs." CIIA. 2009.

[2] Taton, and J. O. Lachaud "Modèle Déformable en Métrique non-euclidienne." Actes du 13ème Congrès Francophone de Reconnaissance des Formes et Intelligence Artificielle (RFIA02) pp. 425-434, 2002.

[3] Geyer, and K. Daniilidis, "Catadioptric projective geometry." International Journal of Computer Vision vol. 45 no. 3, pp 223-243, 2001.

[4] E-M. Mouaddib. "La Vision Omnidirectionnelle, " In Journées nationales de la recherche en robotique, JNRR'05, Guidel, France, Octobre 2005.

[5] I. Bogdanova, X. Bresson, J. P. Thiran, and P. Vandergheynst, "Scale space analysis and active contours for omnidirectional images." Image Processing, IEEE Transactions on, vol. 16 no. 7, pp. 1888-1901, 2007.

[6] J. Denzler, and H. Niemann, "Evaluating the performance of active contour models for real-time object tracking." Asian Conference on Computer Vision. Vol. 2. 1995.

[7] J. Santos-Victor and G. Sandini, "Uncalibrated obstacle detection using normal flow", Machine Vision and Applications, vol. 9, pp. 130-137, 1996.

[8] L. D. Cohen, "On active contour models and balloons." CVGIP: Image understanding vol. 53, no 2,pp 211-218, 1991.

[9] M. Kass, A. Witkin, and D. Terzopoulos, "Snakes: Active contour models." International journal of computer vision, vol. 55, pp. 321-331, 1988.

[10] N. Ohnishi and A. Imiya, "Dominant plane detection from optical flow for the robot navigation", Pattern Recognition Let-ters, vol. 27, pp. 1009-1021, 2006.

[11] P. Merveilleux, O. Labbani-Igbida, and E-M. Mouaddib, "Real-time free space detection and navigation using omnidirectional vision and parametric and geometric active contours." Robotics and Automation (ICRA), 2011 IEEE International Conference on. IEEE, 2011.

[12] P. Merveilleux, O. Labbani-Igbida, and E-M. Mouaddib, "Robust free space segmentation using active contours and monocular omnidirectional vision." Image Processing (ICIP), 2011 18th IEEE International Conference on. IEEE, 2011

[13] T. F. Cootes, C. J. Taylor, D. H. Cooper and J. Graham "Active shape models-their training and application." Computer vision and image understanding Vol. 61 no 1, pp. 38-59, 1995.

[14] Y. EL OMARY, "Modeles deformables et multiresolution pour la détection de contours en traitement d'images. Thèse de doctorat." Université Joseph-Fourier-Grenoble I, 1994.